Nanoscale

Hypoxia-Induced Biosynthesis of Gold Nanoparticles in the Living Brain

Journal:	*Nanoscale*
Manuscript ID	NR-COM-07-2019-005794.R1
Article Type:	Communication
Date Submitted by the Author:	23-Aug-2019
Complete List of Authors:	Rozhkova, Elena; Argonne National Laboratory, NanoBio Interface Group Lee, Byeongdu; Argonne National Laboratory, X-ray Sciences Division Prasad, Judy; University of Chicago Liu, Yuzi; Argonne national Laboratory, Center for Nanoscale Materials Shevchenko, Elena; Argonne National Laboratory, Center for Nanoscale Materials

COMMUNICATION

100Received 00th July 5 2019,
Accepted 00th 2019

DOI: 10.1039/x0xx00000x

Hypoxia-Induced Biosynthesis of Gold Nanoparticles in the Living Brain

Elena A. Rozhkova,[a] Byeongdu Lee,[b] Judy A. Prasad,[c] Yuzi Liu,[a] Elena V. Shevchenko[a]

While a large number of studies deal with biomedical applications of various types of nanoparticles synthetized using wet chemistry, we propose the concept of targeted biosynthesis of nanoparticles in the living brain. Here we demonstrate that the pathological biochemical process of accumulation of reduced pyridine nucleotides under deleterious conditions of the brain hypoxia can be redirected to drive biosynthesis of biocompatible Au nanoparticles from a precursor salt *in-situ* in the immediate vicinity of the hypoxia site, thereby restoring the redox status of the brain.

Hypoxia, or lack of oxygen, leads to disruption and cessation of all vital energetic and metabolic pathways, which is equivalent to a death sentence for cells, tissues and organs. The brain is particularly sensitive organ to oxygen depletion with irreversible changes occurring within a minute.[1] Representing only 2% of the body weight, the brain consumes about 15% of all blood pumped by the heart, and 20% of the total oxygen supply to the body.[2] One of the most life-threatening diseases mediated by hypoxia is stroke.[3] First described by the father of medicine Hippocrates more than 2,400 years ago, stroke or "brain attack" remains one of the main causes of global mortality. For example, in the US it kills someone every four minutes.[4]

Although underlying causes for oxygen deprivation in the brain can be various, and the mechanisms of the brain injury by hypoxia are quite complex and not completely understood, the distinctive hallmarks of this pathology are well-established. These include suppression of electron transfer pathways, impaired adenosine triphosphate (ATP) levels,[5] deficiency of oxidized forms of nicotinamide adenine dinucleotide (NAD) cofactor and, accordingly, increasing in NADH/NAD^+ ratio,[6] which leads to excessive production of reactive oxygen species (ROS), reactive nitrogen species (RNS) and induction of programmed cell death, or apoptosis.[5] NAD^+, discovered in 1906, recently regain a significant attention as a result of recognizing its role in supporting essential bioenergy processes.[7-9]

Under healthy conditions, NAD co-enzymes play an important role in the brain energetics and function, including neurotransmission, learning and memory.[2, 7] Severe hypoxia in the brain can lead to more than 200% increase in the concentration of NADH.[6] Such a morbid accumulation of the reduced form of this cofactor during hypoxia activates enzymes such as NADH-dependent oxidases and nitric oxide synthases (e.g. iNOS) and, consequently, neuronal tissue breakdown and the brain injury by ROS and RNS. Existing anti-hypoxia medicinal treatments can be aimed at interfering one or another specific pathologic pathways, however a more universal approach to combating hypoxia remains challenging.

Nanoparticles (NPs) are extensively studied for their applications in biomedicine for therapy and diagnostics.[10-17] Moreover, NPs can be used for neuroprotection. [18-21] However, most studies focus on the use of pre-synthetized NPs. NP's functionality is related to their physical properties, for example, their ability to interact with external stimuli, such as photons, magnetic field, temperature, pH, sound, and their ability to provide a surface for the delivery of desired molecules, such as polypeptides, DNA, contrasting and therapeutic agents, to target sites.[17] *However, what if we use the complex nature of redox biological processes to synthetize NPs in situ, and this synthesis is triggered only by specific molecules or occurs when concentrations of certain species reach levels that are harmful for cells?*

Here we propose to utilize a strong electron donating ability of NADH cofactor (-320 mV/ NHE) to drive biosynthesis of Au NPs from corresponding precursor *in situ* in the living brain under hypoxia conditions, as depicted in Figure 1a. An excess of reducing equivalents accumulated near the hypoxia site can be redirected to the metal ion reduction reaction, while the formed oxidized NAD^+ became available to serve as a strong electron sink to restore the normal physiological NADH/NAD^+ ratio and cellular respiration, and ultimately help protect the brain. Au-based nanostructures are very appealing for biomedical applications owing to their high biocompatibility and *in vivo* stability.[16, 22-24] Moreover, the inherent antioxidant properties of Au NPs[25] as various ROS scavengers[26-28] add remarkable value to their tissues protection potential.

First, we conducted *ex situ* experiments to prove that NADH can indeed reduce gold precursors resulting in the formation of Au NPs. $AuCl_3$ was chosen as a precursor due to its higher electron sinking capacity of Au (III) and aqueous solution stability compared to Au(I), which in itself can transform into

[a] *Center for Nanoscale Materials, Argonne National Laboratory, 9700 South Cass Avenue, Lemont, Illinois 60439, United States. E-mail: rozhkova@anl.gov shevchenko@anl.gov*
[b] *X-ray Science Division, Argonne National Laboratory, 9700 South Cass Avenue, Lemont, Illinois 60439, United States*
[c] *Department of Neurology, the University of Chicago, 947 E. 58th St., Chicago, IL 60637, United States*

Electronic Supplementary Information (ESI) available online. See DOI: 10.1039/x0xx00000x

Au(III) *in vivo.* [24] Since NADH absorbs light at 340 nm while its oxidized form does not,[29] and Au NPs exhibit plasmon resonance at 520 nm, we monitored the reaction spectroscopically by acquiring the UV-vis spectra.

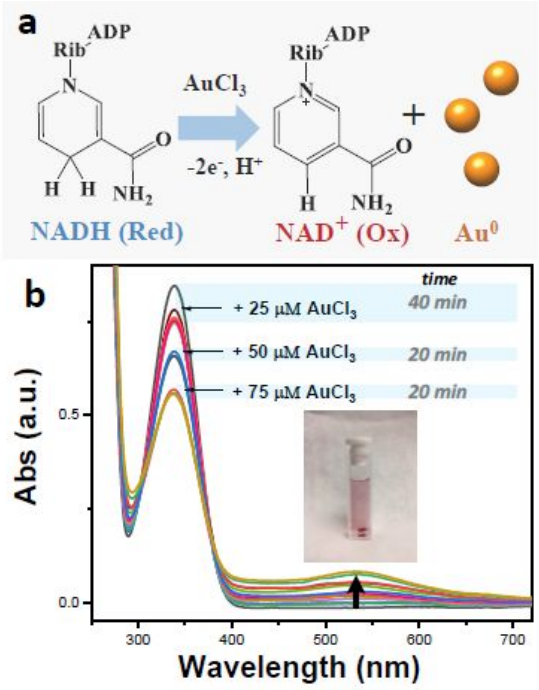

Figure 1. (a) Reaction scheme depicting the transformation of $AuCl_3$ into Au^0 NPs by NADH. Rib-ADP stands for adenosine diphosphate-ribose moiety. (b) Evolution of the UV-vis spectra of NADH upon addition of $AuCl_3$. The molar ratios of $AuCl_3$ to NADH were 1:4, 1:2 and 3:2 upon first, second and third introductions of $AuCl_3$ solution into 100 **µ**M NADH solution. After additions of 25, 50 and 75 µM $AuCl_3$ aliquots, the reaction was allowed for 40, 20 and 20 min, and monitored by recording of 11 UV-vis spectra. The inset in (b) shows the cuvette with synthetized Au NPs.

The introduction of $AuCl_3$ into cuvette containing NADH aqueous solution ($AuCl_3$/NADH molar ratio is 1:4) results in the immediate drop of the intensity of peak at 340 nm indicating the oxidation of NADH (Figure 1b). However, a new peak at 520 nm, characteristic for Au NPs appears after ~7 min of the reaction, and it continues to develop steadily. Interestingly, the further growth of NPs is accompanied by a minor oxidation of NADH as evidenced by only a slight change in the peak intensity at 340 nm in the UV-vis spectra. After 20 min of the reaction, a pink color can be detected by naked eye (Figure 1b, inset). Further additions of $AuCl_3$ to the reaction media are also accompanied by an immediate decrease of the absorbance at 340 nm followed by a slowdown of the NADH oxidation until reaching a plateau. The oxidation of each NADH molecule results in the release of two electrons, whereas three electrons are required to reduce the Au^{3+} ion to Au^0. Based on observations summarized in Figure 1b, it can be assumed that the formation of the NP is influenced not only by the stoichiometry of the NADH and Au NPs precursor. The Au NPs formation appears to be a complex dynamic process where NADH provides the initial trigger for reduction of the metal ion and particle nucleation, and then, possibly, other simultaneous processes, e.g. metal-ligand complex formation, particle-precursor, particle-particle interactions, and particle-catalyzed NADH oxidation,[30] can take place.

It is worth noting that we also tested other types of gold precursors. While AuCl behaved similar to the $AuCl_3$ and was reduced by NADH to Au^0, biocompatible gold-thiolate complexes such as auranofin, solganal and myochrysine known for their use in chrysotherapy,[24] being mixed with NADH yielded no Au NPs that can be attributed to high stability of the gold-thiolate bond under test conditions. However, the formation of Au NPs from gold-thiolate precursors cannot be ruled out *in vivo*, since weak covalent gold-thiolate bond (dissociation energy 50 kJ/mol - 100 kJ/mol) can be successfully reduced in the intracellular microenvironment, liberating gold ions.[31]

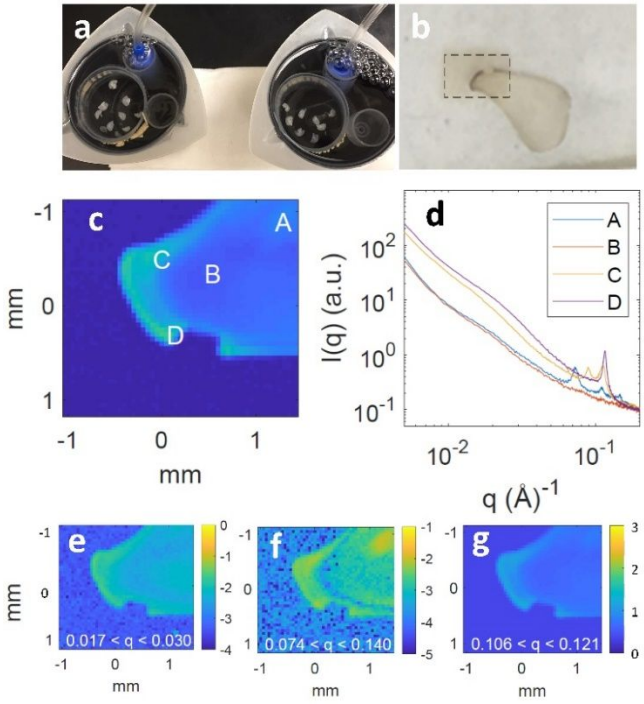

Figure 2. Photographs of the 450 µm brain slices from two mice undergoing oxygenation prior to induction of hypoxia (a). The integrated SAXS intensities were obtained for the 4.5x4.5 mm area in the hypoxic brain section treated with Au (III) precursor (b) pinpointed as A, B, C and D within the 4.5x4.5 mm region (c). The plot shows SAXS curves at four representative positions (d). Figures e, f and g demonstrate the integrated SAXS intensities in the selected q ranges (). The color bars visualize the X-ray scattering intensities (here in log10 scale) with the brighter color corresponding to the stronger scattering intensity.

Encouraged by the results of the *ex situ* experiments, we turned to an experimental animal living brain model in order to test the applicability of our idea *ex vivo.* Coronal 450 µm thick sections of the mouse brain were isolated and prepared by a technique that allows maintaining the integrity of the isolated brain functions for sufficient experimental time-lapse, as depicted in Figure S1.[32] The prepared living brain slices were incubated in a chamber with oxygenated artificial cerebrospinal fluid (ACSF) solution for 40 min maintained at 32-36°C before hypoxia was induced by disabling the

oxygen supply for 2 min, Figure S1. Solution containing Au(III) precursor was applied to the right hemisphere of the brain section, while the left hemisphere was used as an untreated control. In addition, normally oxygenated brain sections were also exposed to the Au(III) precursor for comparison with hypoxic slices. After 5 min incubation with Au(III) precursor, the brain slices were thoroughly washed to insure the removal of the excess of precursors and then fixed with mixture of 2% glutaraldehyde and paraformaldehyde. Only slices that underwent hypoxia and were treated with $AuCl_3$ treatment revealed staining localized mainly in the outer regions of the brain section that is indicative to the presence of Au NPs. In order to confirm the formation of Au NPs we conducted simultaneous small and wide angle X-ray scattering (SAXS and WAXS, respectively) measurements. SAXS allows determining size, shape, size distribution and structural features of nanoscale inorganic[33, 34] and biological species, including complex tissue as the brain,[35] while WAXS determines the crystalline structure of the inorganic particles.

Figure 2 shows the integrated SAXS intensities in the broad q range and more narrow, feature-specific q regions. The SAXS patterns measured at A, C, and D positions and shown in Figure 2c demonstrate peaks at q ~ 0.1 A^{-1}, that can be characteristic for the cell membranes;[35] while no such peaks are detected at position B. The mapping result for this region is presented in Figure 2f. Gold scattering is strong mostly at C and D positions that represents the outer areas of the brain that are stained by pink color. SAXS scattering peak indicating the presence of Au NPs at q~0.027 A^{-1} allows estimating the size of Au NPs as 23.31 nm (~2*pi/0.027).[33, 36] However, the intensity of the WAXS signals was rather weak.

In order to enhance the intensities of the SAXS/WAXS signals, we increased the concentration of Au(III) precursor by 100 times (up to 10mM). Again, the formation of Au NPs took place only in hypoxic brain slices (Figure S2). The data obtained for hypoxic brain slices treated with higher Au(III) concentration are shown in Figure 3. The plots of SAXS intensities in the range corresponding to the formed NPs and WAXS integrated intensities of (111) reflection of Au shows a strong correlation (Figures 3b and 3c, respectively). The concentration of Au NPs is higher in the outer areas of the brain slice. The size of the Au NPs, estimated by the position of the peak on the SAXS spectrum was about ~10 nm. Au NPs biosynthesized *in situ* in the hypoxic brain were isolated from the brain slices and visualized using the TEM. As demonstrated in Figures 3d and 3e, biosynthetized Au NPs are spherical and ~10 nm in diameter that is consistent with the SAXS data.

Note, that in studies with lower and higher concentrations of the Au (III) precursor, the brains of different animals were used. Although the procedures for preparation and treatment of the brain for both animals were standard, and the difference in the size of biosynthesized Au nanoparticles can be explained by the difference in the initial concentration of Au (III) precursor, the influence of individual characteristics in biochemistry and anatomy of each animal cannot be excluded.

The Au NPs were formed only in the brain slices that underwent hypoxia. No Au NPs was detected in the presence of Au(III) precursor in the oxygenated brain slices. The SAXS/WAXS data on hypoxic brain treated with different Au(III) salt concentrations prove the formation of Au NPs. In both cases, the formation of Au NPs is localized closer to the surface of mouse brain while the sizes of particles at the surface and inner brain are the same. This observation indicates that all Au NPs nucleated and grew almost at the same time and this was mediated by the processes caused by hypoxia in the living brain.

The density of Au NPs distribution was less pronounced within the white matter regions of the brain (Figure 3f) where tightly-packed lamellar structures material can be found[35] as it is evidenced by SAXS/WAXS data (Figures 3f-3i). This result is expected since white matter contains myriads of axons, elongated neural cell "tails", which function as an electrical circuit connecting neurons, but are less involved in the NADH/NAD^+ redox processes in the cell's body. Consequently, the probability of the formation of Au NPs in this tightly packed brain tissue is significantly lower due to poorer permeability to the precursor, on the one hand, and less sensitivity to hypoxia, on the other.

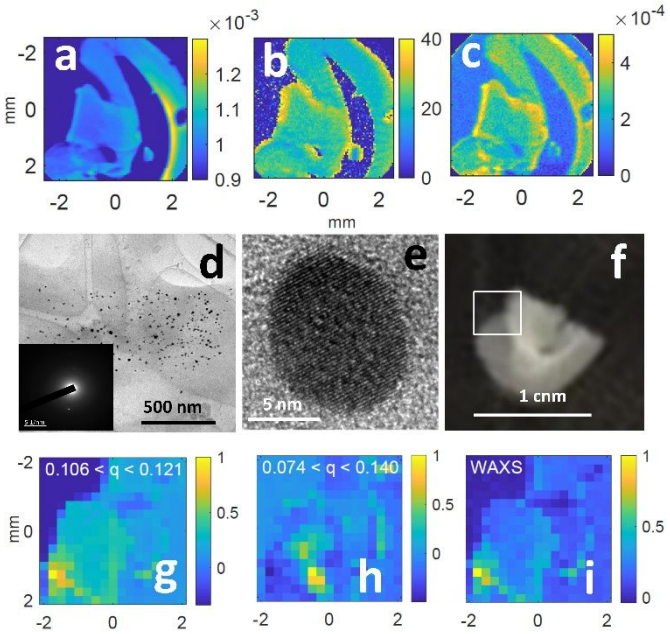

Figure 3. Integrated SAXS intensities maps (a) obtained for hypoxic 450 µm-thick brain slice treated with 10mM (x100 times higher concentration) of Au(III) precursor as compared to data shown in Figure 2. Plots of SAXS intensities in the selected (0.075-0.14) q range (b) and WAXS integrated intensities of (111) reflection of Au (c). The representative TEM (d) and higher magnification TEM (e) images of the *in-situ* biosynthesized Au NPs. The inset in (d) shows the SAED pattern corresponding to the area shown in (f). Optical image of the brain slice containing higher amount of the white matter (f) and corresponding integrated SAXS intensities maps for selected q ranges (g, h). WAXS integrated intensities (i) of (111) reflection of Au obtained for section of the brain shown in the white square in (f). The colour bars represent the X-ray scattering intensities, where the brighter colour corresponds to a stronger scattering intensity.

Biosynthesis of NPs is a striking phenomenon in nature. Inspiring examples include storage and transport of iron atoms in a non-toxic form of ferric oxyhydroxide cluster in the ferritin protein cage, [37] using metal salts as terminal sinks in electron transfer pathways and formation of metal particles by bacteria,[38-40] and biomineralization of magnetite nanocrystals in specific organelle magnetosome that enables coordinated movement of magnetotactic bacteria.[41] Under certain experimental conditions, metal complexes and nanoclusters can be obtained in mammalian cells or in a whole animal, mainly for use in imaging.[42-48] However,

the mechanisms of these bio-synthesis are often spontaneous, poorly understood and, therefore, difficult to control. In our approach, a pathological process initiates and controls biosynthesis of biocompatible Au nanoparticles from precursor salts in the immediate vicinity of the hypoxia site, thereby restoring the redox status of the brain.

Conclusions

Here we demonstrated a proof of a concept – redirection of the pathological biochemical process of accumulation of reduced pyridine nucleotides under deleterious hypoxia conditions in the brain toward the reduction of the precursor salt and biosynthesis of biologically compatible, antioxidant Au^0 NPs and the simultaneous restoring of the tissue redox status. The proposed concept of biosynthesis of Au NPs triggered by misbalance of the cellular pathological process (here by hypoxia), can complement the more classical uses of pre-synthetized Au NPs, as popular diagnostic imaging and therapeutic NP agents.[24, 49]

This approach can be implemented in other highly metabolic tissues and organs that are particularly vulnerable to oxygen deficiencies, such as heart, kidney and liver.[50] Besides, combined with innovative technologies for preserving and restoring the functions of isolated tissue at ambient conditions,[51] in situ biosynthesis of nanosized materials, in particular Au NPs can be utilized in organs recovery and transplantation. In addition, our approach can be valuable for combinatorial screening of antihypoxia therapeutics on isolated sections of the living brain, as well as for detection of abnormally elevated levels of the reducing equivalents NAD(P)H in cells and isolated tissues.

Materials and Methods

Gold (III) chloride ($AuCl_3$), cofactors NADH, NADPH and ATP were from Sigma/Aldrich. Paraformaldehyde/glutarldehyde fixative solution was from the Electron Microscopy Sciences. Gold NPS were formed through reduction of the $AuCl_3$ by cofactors. Briefly, 100 µM NADH solution in PBS, pH 7.4, was placed in a cuvette and mixed with aliquots of $AuCl_3$ in the same buffer to achieve 4:1, 2:1, and equimolar NADH/precursor ratios, at room temperature under constant stirring. Oxidation of NADH and formation of Au NPs were recorded at 340 nm and 520 nm, respectively, by UV-vis spectra using CARY-50 spectrophotometer.

Animal care and living acute brain sections preparation

All animal care procedures and the brain slice preparation procedures were approved by the Institutional Animal Care and Use Committee (IACUC) at the University of Chicago in accordance with federal regulations issued by the U.S. Department of Agriculture and the National Institutes of Health Office of Laboratory Animal Welfare. Four to five animals per cage were maintained in a pathogen-free animal facility, received standard laboratory rodent food and water *ad libitum.* Experimental mice C57BL/6J (male, 17 days old, n=2) were anesthetized by intraperitoneal injection of ketamine-xylazine. After anaesthetic level was confirmed, mice were quickly decapitated, and their brains were promptly removed. Brains from two mice were used that allowed obtaining a total of 32 brain slices. The brains were placed to the ice-cold "cut" aCSF solution (containing the following, in mM: 3 KCl, 26 NaHCO3, 1 NaH_2PO_4, 0.5 CaCl2, 3.5 $MgSO_4$ 25 dextrose, 123 sucrose) for quick, less than 5 min, slicing on vibratome at a thickness of 450 µm. The sections then were placed into an oxygenated incubation ACSF solution (containing the following, in mM: 123 NaCl, 3 KCl, 26 $NaHCO_3$, 1 NaH_2PO_4, 2 CaCl2, 6 $MgSO_4$, 25 dextrose) for 40 min, maintained at 32-36°C.[32] Tissue was left to rest at room temperature for 30 min before hypoxic induction. Hypoxia was induced in brain slices in an oxygen-deprived chamber for 5 min, while their opposite hemisphere counterparts were used as normally oxygenated controls.

***In-situ* Au NPs Biosynthesis**

Aliquots of aqueous $AuCl_3$ were added to oxygen-deprived and oxygenated (control) brain slices to reach 100µM-10mM final concentrations of the precursor, incubated for 5 min, thoroughly rinsed (to ensure removal of precursor excess), and fixed using 2% glutaraldehyde + 2% paraformaldehyde in 0.1M phosophate buffer, pH 7.4, and then stored in the same fixing solution at +5°C before imaging and analyses. The experiments with different concentrations of $AuCl_3$ were performed on brain slices of two animals.

Synchrotron SAXS and WAXS analyses

Before the beam experiment brain slices were removed from the solution, and mounted by sealing them between two thin glass cover slides (Fisherfinest). In situ SAXS/WAXS measurement was carried out at beamline 12-ID-B of the Advanced Photon Source (APS), Argonne National Laboratory. In situ SAXS data were analysed by custom-built software that is run on Matlab after standard data correction including background correction.

TEM Imaging

To isolate Au NPs fixed brain slices were freeze-dried, mechanically grinded down, and then the NPs were extracted by DI water followed by separation of the biological debris *via* centrifugation (2000 rpm for 10 min). The NPs-containing supernatant was dropped onto Ultrathin Carbon Cu TEM grid with the Formvar pre-removed in toluene, the samples were allowed to set for ~1 hour and then rinsed by DI water. TEM analysis of the NPs was performed with a JEM-2100F operated at 200 kV.

Acknowledgment.

This work was performed at the Center for Nanoscale Materials, a U.S. Department of Energy, Office of Science, Office of Basic Energy Sciences User Facility under Contract No. DE-AC02-06CH11357. We thank Prof. Jason MacLean (Department of Neurobiology University of Chicago) for encouraging discussion and help in experiments on live brain.

Conflicts of interest

There are no conflicts to declare.

Notes and references

1. K. G. Alberti, *J Clin Pathol Suppl (R Coll Pathol)*, 1977, **11**, 14-20.

2. P. J. Magistretti and L. Pellerin, *Ann N Y Acad Sci*, 1996, **777**, 380-387.
3. A. P. Coupland, A. Thapar, M. I. Qureshi, H. Jenkins and A. H. Davies, *J R Soc Med*, 2017, **110**, 9-12.
4. E. J. Benjamin, M. J. Blaha, S. E. Chiuve, M. Cushman, S. R. Das, R. Deo, S. D. de Ferranti, J. Floyd, M. Fornage, C. Gillespie, C. R. Isasi, M. C. Jimenez, L. C. Jordan, S. E. Judd, D. Lackland, J. H. Lichtman, L. Lisabeth, S. Liu, C. T. Longenecker, R. H. Mackey, K. Matsushita, D. Mozaffarian, M. E. Mussolino, K. Nasir, R. W. Neumar, L. Palaniappan, D. K. Pandey, R. R. Thiagarajan, M. J. Reeves, M. Ritchey, C. J. Rodriguez, G. A. Roth, W. D. Rosamond, C. Sasson, A. Towfighi, C. W. Tsao, M. B. Turner, S. S. Virani, J. H. Voeks, J. Z. Willey, J. T. Wilkins, J. H. Wu, H. M. Alger, S. S. Wong, P. Muntner, C. American Heart Association Statistics and S. Stroke Statistics, *Circulation*, 2017, **135**, e146-e603.
5. K. M. Busl and D. M. Greer, *NeuroRehabilitation*, 2010, **26**, 5-13.
6. O. Garofalo, D. W. Cox and H. S. Bachelard, *J Neurochem*, 1988, **51**, 172-176.
7. W. H. Ying, *Front Biosci-Landmrk*, 2007, **12**, 1863-1888.
8. H. B. Zhang, D. Ryu, Y. B. Wu, K. Gariani, X. Wang, P. L. Luan, D. D'Amico, E. R. Ropelle, M. P. Lutolf, R. Aebersold, K. Schoonjans, K. J. Menzies and J. Auwerx, *Science*, 2016, **352**, 1436-1443.
9. A. P. Gomes, N. L. Price, A. J. Y. Ling, J. J. Moslehi, M. K. Montgomery, L. Rajman, J. P. White, J. S. Teodoro, C. D. Wrann, B. P. Hubbard, E. M. Mercken, C. M. Palmeira, R. de Cabo, A. P. Rolo, N. Turner, E. L. Bell and D. A. Sinclair, *Cell*, 2013, **155**, 1624-1638.
10. E. A. Rozhkova, *Adv Mater*, 2011, **23**, H136-H150.
11. E. A. Vitol, V. Novosad and E. A. Rozhkova, *Nanomedicine-Uk*, 2012, **7**, 1611-1624.
12. J. Lee, A. C. Gordon, H. Kim, W. Park, S. Cho, B. Lee, A. C. Larson, E. A. Rozhkova and D. H. Kim, *Biomaterials*, 2016, **109**, 69-77.
13. D. H. Kim, E. A. Vitol, J. Liu, S. Balasubramanian, D. J. Gosztola, E. E. Cohen, V. Novosad and E. A. Rozhkova, *Langmuir*, 2013, **29**, 7425-7432.
14. E. A. Vitol, E. A. Rozhkova, V. Rose, B. D. Stripe, N. R. Young, E. E. W. Cohen, L. Leoni and V. Novosad, *Adv Mater Interfaces*, 2014, **1**.
15. D. H. Kim, E. A. Rozhkova, T. Rajh, S. D. Bader and V. Novosad, *Ieee T Magn*, 2009, **45**, 4821-4824.
16. M. U. Farooq, V. Novosad, E. A. Rozhkova, H. Wali, A. Ali, A. A. Fateh, P. B. Neogi, A. Neogi and Z. M. Wang, *Sci Rep-Uk*, 2018, **8**.
17. K. McNamara and S. A. M. Tofail, *Adv Phys-X*, 2017, **2**, 54-88.
18. C. K. Kim, T. Kim, I. Y. Choi, M. Soh, D. Kim, Y. J. Kim, H. Jang, H. S. Yang, J. Y. Kim, H. K. Park, S. P. Park, S. Park, T. Yu, B. W. Yoon, S. H. Lee and T. Hyeon, *Angew Chem Int Edit*, 2012, **51**, 11039-11043.
19. A. Y. Estevez, S. Pritchard, K. Harper, J. W. Aston, A. Lynch, J. J. Lucky, J. S. Ludington, P. Chatani, W. P. Mosenthal, J. C. Leiter, S. Andreescu and J. S. Erlichman, *Free Radical Bio Med*, 2011, **51**, 1155-1163.
20. K. L. Heckman, W. DeCoteau, A. Estevez, K. J. Reed, W. Costanzo, D. Sanford, J. C. Leiter, J. Clauss, K. Knapp, C. Gomez, P. Mullen, E. Rathbun, K. Prime, J. Marini, J. Patchefsky, A. S. Patchefsky, R. K. Hailstone and J. S. Erlichman, *Acs Nano*, 2013, **7**, 10582-10596.
21. H. J. Kwon, M. Y. Cha, D. Kim, D. K. Kim, M. Soh, K. Shin, T. Hyeon and I. Mook-Jung, *Acs Nano*, 2016, **10**, 2860-2870.
22. D. A. Giljohann, D. S. Seferos, W. L. Daniel, M. D. Massich, P. C. Patel and C. A. Mirkin, *Angew Chem Int Edit*, 2010, **49**, 3280-3294.
23. C. J. Murphy, A. M. Gole, J. W. Stone, P. N. Sisco, A. M. Alkilany, E. C. Goldsmith and S. C. Baxter, *Accounts Chem Res*, 2008, **41**, 1721-1730.
24. A. S. Thakor, J. Jokerst, C. Zavaleta, T. F. Massoud and S. S. Gambhir, *Nano Lett*, 2011, **11**, 4029-4036.
25. L. Valgimigli, A. Baschieri and R. Amorati, *J Mater Chem B*, 2018, **6**, 2036-2051.
26. K. Esumi, N. Takei and T. Yoshimura, *Colloid Surface B*, 2003, **32**, 117-123.
27. W. W. He, Y. T. Zhou, W. G. Warner, X. N. Hu, X. C. Wu, Z. Zheng, M. D. Boudreau and J. J. Yin, *Biomaterials*, 2013, **34**, 765-773.
28. J. N. Li, W. Q. Liu, X. C. Wu and X. F. Gao, *Biomaterials*, 2015, **48**, 37-44.
29. E. A. Rozhkova, N. Fujimoto, I. Sagami, S. N. Daff and T. Shimizu, *J Biol Chem*, 2002, **277**, 16888-16894.
30. X. H. Huang, I. H. El-Sayed, X. B. Yi and M. A. El-Sayed, *J Photoch Photobio B*, 2005, **81**, 76-83.
31. Y. R. Xue, X. Li, H. B. Li and W. K. Zhang, *Nature Communications*, 2014, **5**.
32. A. J. Sadovsky and J. N. MacLean, *J Neurosci*, 2013, **33**, 14048-U14676.
33. T. Li, A. J. Senesi and B. Lee, *Chem Rev*, 2016, **116**, 11128-11180.
34. S. G. Kwon, G. Krylova, P. J. Phillips, R. F. Klie, S. Chattopadhyay, T. Shibata, E. E. Bunel, Y. Z. Liu, V. B. Prakapenka, B. Lee and E. V. Shevchenko, *Nat Mater*, 2015, **14**, 215-223.
35. N. Yagi, *J Phys Conf Ser*, 2011, **272**.
36. H. Borchert, E. V. Shevchenko, A. Robert, I. Mekis, A. Kornowski, G. Grübel and H. Weller, *Langmuir*, 2005, **21**, 1931-1936.
37. J. Seckback, *J Plant Nutr*, 1982, **5**, 369-394.
38. F. Caccavo, D. J. Lonergan, D. R. Lovley, M. Davis, J. F. Stolz and M. J. Mcinerney, *Appl Environ Microb*, 1994, **60**, 3752-3759.
39. B. A. Methe, K. E. Nelson, J. A. Eisen, I. T. Paulsen, W. Nelson, J. F. Heidelberg, D. Wu, M. Wu, N. Ward, M. J. Beanan, R. J. Dodson, R. Madupu, L. M. Brinkac, S. C. Daugherty, R. T. DeBoy, A. S. Durkin, M. Gwinn, J. F. Kolonay, S. A. Sullivan, D. H. Haft, J. Selengut, T. M. Davidsen, N. Zafar, O. White, B. Tran, C. Romero, H. A. Forberger, J. Weidman, H. Khouri, T. V. Feldblyum, T. R. Utterback, S. E. Van Aken, D. R. Lovley and C. M. Fraser, *Science*, 2003, **302**, 1967-1969.
40. J. F. Heidelberg, I. T. Paulsen, K. E. Nelson, E. J. Gaidos, W. C. Nelson, T. D. Read, J. A. Eisen, R. Seshadri, N. Ward, B. Methe, R. A. Clayton, T. Meyer, A. Tsapin, J. Scott, M. Beanan, L. Brinkac, S. Daugherty, R. T. DeBoy, R. J. Dodson, A. S. Durkin, D. H. Haft, J. F. Kolonay, R. Madupu, J. D. Peterson, L. A. Umayam, O. White, A. M. Wolf, J. Vamathevan, J. Weidman, M. Impraim, K. Lee, K. Berry, C. Lee, J. Mueller, H. Khouri, J. Gill, T. R. Utterback, L. A. McDonald, T. V. Feldblyum, H. O. Smith, J. C. Venter, K. H.

Nealson and C. M. Fraser, *Nat Biotechnol*, 2002, **20**, 1118-1123.
41. R. Blakemore, *Science*, 1975, **190**, 377-379.
42. J. Jin, T. Liu, M. Li, C. Yuan, Y. Liu, J. Tang, Z. Feng, Y. Zhou, F. Yang and N. Gu, *Colloids Surf B Biointerfaces*, 2018, **163**, 385-393.
43. J. Ye, J. L. Wang, Q. W. Li, X. W. Dong, W. Ge, Y. Chen, X. R. Jiang, H. D. Liu, H. Jiang and X. M. Wang, *Biomater Sci-Uk*, 2016, **4**, 652-660.
44. J. L. Wang, G. Zhang, Q. W. Li, H. Jiang, C. Y. Liu, C. Amatore and X. M. Wang, *Sci Rep-Uk*, 2013, **3**.
45. C. Pilapong, S. Pongpiajun and S. Mankhetkorn, *Mater Lett*, 2015, **140**, 162-165.
46. S. P. Gao, D. H. Chen, Q. W. Li, J. Ye, H. Jiang, C. Amatore and X. M. Wang, *Sci Rep-Uk*, 2014, **4**.
47. D. H. Chen, C. Q. Zhao, J. Ye, Q. W. Li, X. L. Liu, M. N. Su, H. Jiang, C. Amatore, M. Selke and X. M. Wang, *Acs Appl Mater Inter*, 2015, **7**, 18163-18169.
48. T. D. Fernandez, J. R. Pearson, M. P. Leal, M. J. Torres, M. Blanca, C. Mayorga and X. Le Guevel, *Biomaterials*, 2015, **43**, 1-12.
49. E. C. Dreaden, A. M. Alkilany, X. Huang, C. J. Murphy and M. A. El-Sayed, *Chemical Society Reviews*, 2012, **41**, 2740-2779.
50. M. T. Tran, Z. K. Zsengeller, A. H. Berg, E. V. Khankin, M. K. Bhasin, W. Kim, C. B. Clish, I. E. Stillman, S. A. Karumanchi, E. P. Rhee and S. M. Parikh, *Nature*, 2016, **531**, 528-+.
51. Z. Vrselja, S. G. Daniele, J. Silbereis, F. Talpo, Y. M. Morozov, A. M. M. Sousa, B. S. Tanaka, M. Skarica, M. Pletikos, N. Kaur, Z. W. Zhuang, Z. Liu, R. Alkawadri, A. J. Sinusas, S. R. Latham, S. G. Waxman and N. Sestan, *Nature*, 2019, **568**, 336-+.